Principal horizontal stress orientations prior to the 2011 M_w 9.0 Tohoku-Oki, Japan, earthquake in its source area

Weiren Lin,[1,2,3] Saneatsu Saito,[4] Yoshinori Sanada,[5] Yuzuru Yamamoto,[4] Yoshitaka Hashimoto,[6] and Toshiya Kanamatsu[4]

Received 28 July 2011; revised 19 August 2011; accepted 19 August 2011; published 15 September 2011.

[1] We determined principal horizontal stress orientations as of 1999 at sites in the source area of the 2011 M_w 9.0 Tohoku-Oki earthquake, on the deep-sea terrace of the Japan Trench. The maximum principal horizontal stress orientation at site 1151 of Ocean Drilling Program Leg 186, located in an aseismic zone, was east-southeast, parallel with the plate convergence direction; and the stress orientation at site 1150 of Leg 186, in a seismically active zone, was south-southeast, suggestive of a local stress feature due to the influence of seismic activity. Aftershocks with normal faulting mechanisms, observed in the hanging wall of the plate interface that ruptured during the Tohoku-Oki earthquake, indicate a normal faulting postseismic stress regime, which clearly differs from the stress state prior to the earthquake. Consequently, the stress state may have changed from a reverse to a normal faulting stress regime during the Tohoku-Oki earthquake sequence. **Citation:** Lin, W., S. Saito, Y. Sanada, Y. Yamamoto, Y. Hashimoto, and T. Kanamatsu (2011), Principal horizontal stress orientations prior to the 2011 M_w 9.0 Tohoku-Oki, Japan, earthquake in its source area, *Geophys. Res. Lett.*, *38*, L00G10, doi:10.1029/2011GL049097.

1. Introduction

[2] Leg 186 of the Ocean Drilling Program (ODP) drilled the forearc basin at two sites in the Sanriku-Oki segment of the Japan Trench during June–August 1999, about 12 years before this segment ruptured in the giant (M_w 9.0) 2011 Tohoku-Oki earthquake [*Shipboard Scientific Party*, 2000a]. The drilling sites are located on the deep-sea terrace of the Japan Trench about 100 km north-northeast of the epicenter of the mainshock, and above the zone of large coseismic slip during the earthquake (Figures 1a and 1b) [*Avouac*, 2011].

[3] Establishing the in situ stress state along active subduction zones before, during, and after a giant earthquake is critical for modeling various coseismic phenomena and for understanding the accumulation and release of seismic energy in the earthquake cycles of giant events, which account for the majority of Earth's seismic energy release. In the source area of the Tohoku-Oki earthquake, many aftershocks were observed with normal faulting mechanisms [*Asano et al.*, 2011]. This observation suggests the possibility of dynamic overshoot during the large shallow slip near the trench [*Ide et al.*, 2011]. To verify stress changes accompanying the earthquake, knowledge of the stress state prior to the earthquake is essential.

[4] An important approach for determining in situ stresses at depth is to directly measure stress by borehole logging, core-based methods, and downhole experiments [*Zoback et al.*, 2003]. The seismogenic parts of plate margins are accessible through the ODP and its successor, the Integrated Ocean Drilling Program (IODP). An IODP proposal to penetrate the fault that ruptured during the Tohoku-Oki earthquake will aim to determine postseismic stress by direct measurements and coseismic stress by frictional heat signals. However, no direct measurements of stress in the Tohoku-Oki subduction zone are available from before the 2011 earthquake.

[5] To obtain the principal horizontal stress orientations before the 2011 earthquake, we analyzed wireline logging Formation MicroScanner (FMS) images and caliper data that were collected during ODP Leg 186 and have not previously been analyzed for this purpose. We successfully determined stress orientations from the azimuths of stress-induced compressive failures (breakouts) and drilling-induced tensile fractures (DITFs).

2. Study Area and Wireline Logging

[6] The main objective of drilling during ODP Leg 186, conducted by the drilling vessel *JOIDES Resolution*, was to investigate the dynamic properties of the active plate subduction zone of the Japan Trench, where the Tohoku-Oki earthquake happened to occur approximately 12 years later.

[7] The convergent margin off northern Honshu is where the oldest Pacific oceanic plate (Cretaceous, >100 Ma) underthrusts the Okhotsk plate in a west-northwest direction at a high rate of 8 cm/y (Figure 1a) [*Avouac*, 2011]. The Japan Trench system consists of a deep-sea terrace, inner trench slope, midslope terrace, trench lower slope, Japan Trench, and outer trench slope [*Shipboard Scientific Party*, 2000a]. A forearc basin developed in the deep-sea terrace and inner trench slope is filled with Neogene sediments as much as 5 km thick (Figure 1c). The two drilling sites (1150 and 1151) on the deep-sea terrace are on the eastern edge of the forearc basin, where the Neogene section is ~1.5 km thick. Sites 1150 (39°11′N, 143°20′E) and 1151 (38°45′N,

[1]Kochi Institute for Core Sample Research, Japan Agency for Marine-Earth Science and Technology, Nankoku, Japan.
[2]Geology Course, Graduate School of Arts and Sciences, Kochi University, Kochi, Japan.
[3]Key Laboratory of Tectonics and Petroleum Resources of Ministry of Education, China University of Geosciences, Wuhan, China.
[4]Institute for Research on Earth Evolution, Japan Agency for Marine-Earth Science and Technology, Yokosuka, Japan.
[5]Center for Deep Earth Exploration, Japan Agency for Marine-Earth Science and Technology, Yokohama, Japan.
[6]Department of Applied Science, Kochi University, Kochi, Japan.

0094-8276/11/2011GL049097

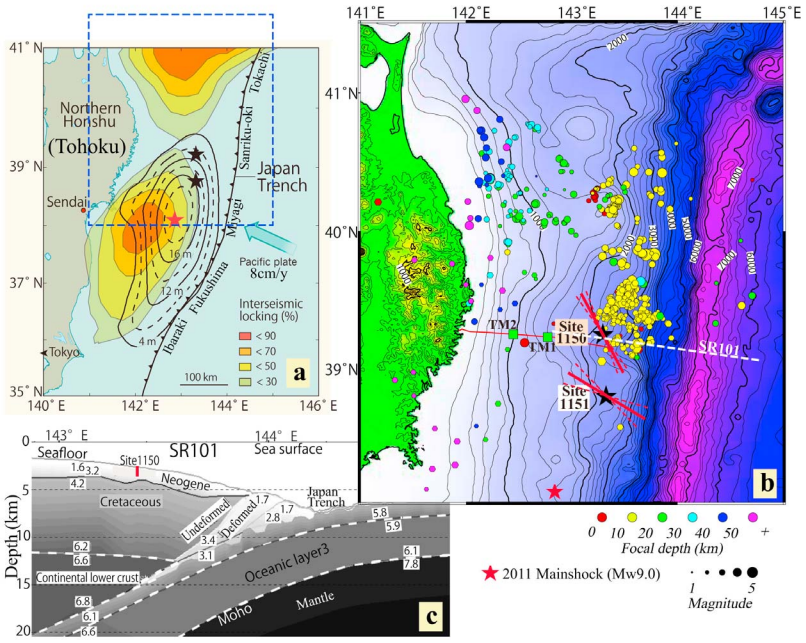

Figure 1. Location and setting of ODP Leg186 drilling sites 1150 and 1151. (a) Locations of the epicenter of the 2011 M_w 9.0 Tohoku-Oki Earthquake mainshock (red star) and the drilling sites (black stars) (modified from *Avouac* [2011]). The earthquake ruptured the plate interface along which the Pacific plate subducts beneath northern Honshu (Okhotsk plate) at a rate of 8 cm/y approximately. Black contour lines analyzed by *Ozawa et al.* [2011] show the coseismic slip displacement which is considerably dependent on models deployed by different researchers for inversion analyses. The color contours show the degree of interplate coupling before the earthquake (interseismic locking). The frame of dashed blue-line shows the area of Figure 1b. (b) Bathymetric map around the drilling sites 1150 and 1151 (black stars) and their maximum principal horizontal stress orientations (modified from *Shipboard Scientific Party* [2000a]). Red lines at the drilling sites show the stress orientations in terms of average azimuth (solid line) and their standard deviations (dashed lines). Two green squares and red line show the TM1 and TM2 ocean-bottom pressure gauges and their connecting cable to shore station which recorded characteristic two-stage tsunami development waveforms [*Maeda et al.*, 2011]. The other symbols show microearthquakes (circles from *Hino et al.* [2000]; hexagons from *Suyehiro and Nishizawa* [1994]). The dashed white line labeled SR101 shows the location of section map in Figure 1c. (c) Interpreted seismic reflection section of off the Sanriku coast through site 1150 (modified from *Tsuru et al.* [2000]). The red line shows drilling interval at site 1150 approximately. Number labels show the P wave velocities.

143°20′E) are 48 km apart, and lie 127 km and 83 km, respectively, north-northeast of the epicenter of the Tohoku-Oki earthquake mainshock (38°06′N, 142°52′E, determined by the Japan Meteorological Agency) (Figure 1b). They are located in areas with contrasting seismic characteristics. Site 1150 is within a seismically active zone where microearthquakes have been frequent and M7 earthquakes are known to recur, and site 1151 is within an aseismic zone where microearthquakes were rare before the drilling (Figure 1b) [*Shipboard Scientific Party*, 2000a].

[8] At each drilling site, four closely spaced boreholes were drilled for coring, logging, and installation of borehole geophysical observation equipment. The boreholes in which wireline logging was carried out at the two sites were 1150B and 1151D. They were drilled vertically to 1182 and 874 meters below seafloor (mbsf) in water depths of 2681 and 2172 m, respectively, penetrating the Neogene forearc basin about 10 km above the gently dipping (<5°) plate boundary (Figure 1c).

[9] After core drilling at borehole 1150B reached the target depth, wireline logging including FMS imaging was carried out. In the first pass (Pass 1), the FMS tool string encountered an obstruction at ~473 mbsf, and the borehole was logged upward from this depth. In the second pass (Pass 2), the logging tool reached the borehole bottom, but logging between 473 and 775 mbsf was incomplete. Both passes were carried out on the same day [*Shipboard Scientific Party*, 2000b]. For borehole 1151D, two FMS logging passes carried out within about 10 hours reached the bottom of the borehole. Because the two FMS loggings were nearly identical, we used only data from Pass 1 in this study.

[10] The FMS tool has four arms at 90° angles, each of which took electrical images (Figure 2b). Because the diameters of the drilling bits were relatively large, 9 7/8 inches (~25 cm) and 11 7/16 inches (~29 cm) for boreholes 1150B and 1151D, respectively, the FMS images covered only about 25% and 21% of the borehole walls (Figure 2). The FMS tool also measured the borehole diameter in two orthogonal directions, serving as a four-arm caliper tool.

[11] Because both breakouts and DITFs are dependent on in situ stress conditions, we can use information on their azimuths to determine orientations of in situ principal stresses in the plane perpendicular to the borehole axis. As breakouts and DITFs both form during or shortly after drilling, they are records of the stress state at the time of drilling. The borehole FMS images enable both the breakouts and DITFs to be identified and the horizontal stress orientations to be determined. In principle, the width (span) of breakouts can con-

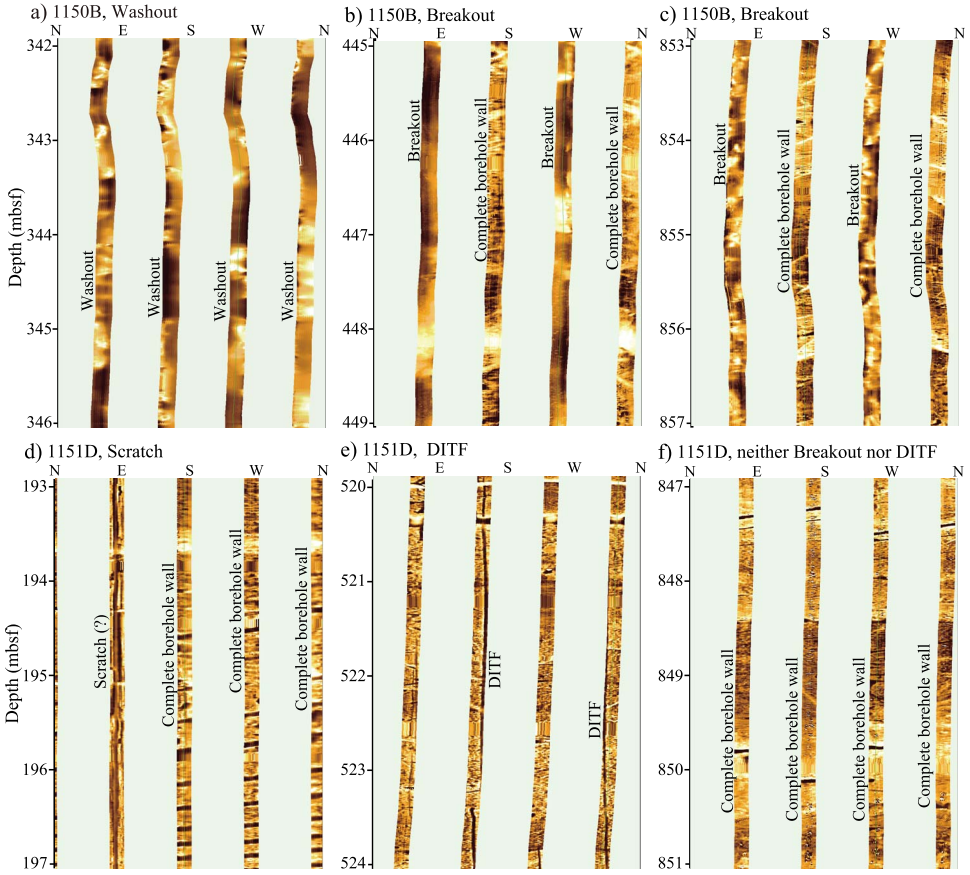

Figure 2. Borehole wall FMS electrical images at boreholes 1150B and 1151D. (a) 1150B, 342–346 mbsf shows washouts. Blank regions between columns are unimaged portions of the borehole wall between the FMS arms. (b) 1150B, 445–449 mbsf. The sharp columns show the formation structures indicating complete borehole wall; unsharp images show borehole wall failure (breakouts). (c) 1150B, 853–857 mbsf shows breakouts. (d) 1151D, 193–197 mbsf shows three columns of complete borehole wall and one damaged side. It indicates that no breakouts occurred although elongation was recognized by caliper data (Figure 3d). (e) 1151D, 520–524 mbsf shows a pair of DITFs. (f) 1151D, 847–851 mbsf shows an example of complete borehole wall.

strain the magnitude of the maximum principal horizontal stress on the basis of the minimum principal horizontal stress magnitude and the rock compressive strength [*Zoback et al.*, 2003]. However, breakout width data were poorly resolved in this study owing to the relatively poor coverage of FMS images. Usually, one pair of caliper arms stops at breakouts (elongations) because their spring forces them into the breakout, making it possible to determine breakout azimuths from caliper data, but that was not possible for DITF data because the tensile fractures were narrower than the caliper pads. For breakout analyses, the caliper data with 6-inch (~15 cm) resolution is superior to statistical calculations. On the other hand, caliper data cannot distinguish stress-induced breakouts from borehole elongation from other causes. Therefore, FMS images are an essential supplement to caliper data, providing direct and visual evidence to characterize breakouts.

3. Stress Orientations From Borehole Breakouts and DITFs

[12] To identify breakouts and determine their azimuth, we observed the FMS images and checked the two borehole diameters in the caliper data to identify breakouts; then we calculated their azimuths which can be interpreted as azimuth of the minimum principal horizontal stresses. We identified DITFs and determined their azimuths from FMS images. The images covered no more than 25% of the borehole wall, thus some DITFs on borehole walls might have been missed.

[13] Breakouts or DITFs should be found in pairs on opposite sides of the borehole wall (180° apart) if the rock strength around the borehole is uniform (homogeneous lithology). DITFs should also be perpendicular to the borehole wall and parallel to the borehole axis in vertical boreholes, hence they should appear to be very straight in FMS images. Breakouts should be also parallel to the borehole axis and wider than fractures and lacking their sharp, straight boundaries. These characteristics were valuable in distinguishing breakouts and DITFs from other borehole wall failures such as washouts and pre-existing structural fractures. Using these criteria, we identified breakouts and DITFs and recorded the azimuth data of DITFs from the FMS images.

3.1. Borehole 1150B

[14] Logging during Pass 1 (171–472 mbsf) penetrated geologic units IB (136–222 mbsf, late Pliocene), IIA (222–424 mbsf, early to late Pliocene), and IIB (424–598 mbsf,

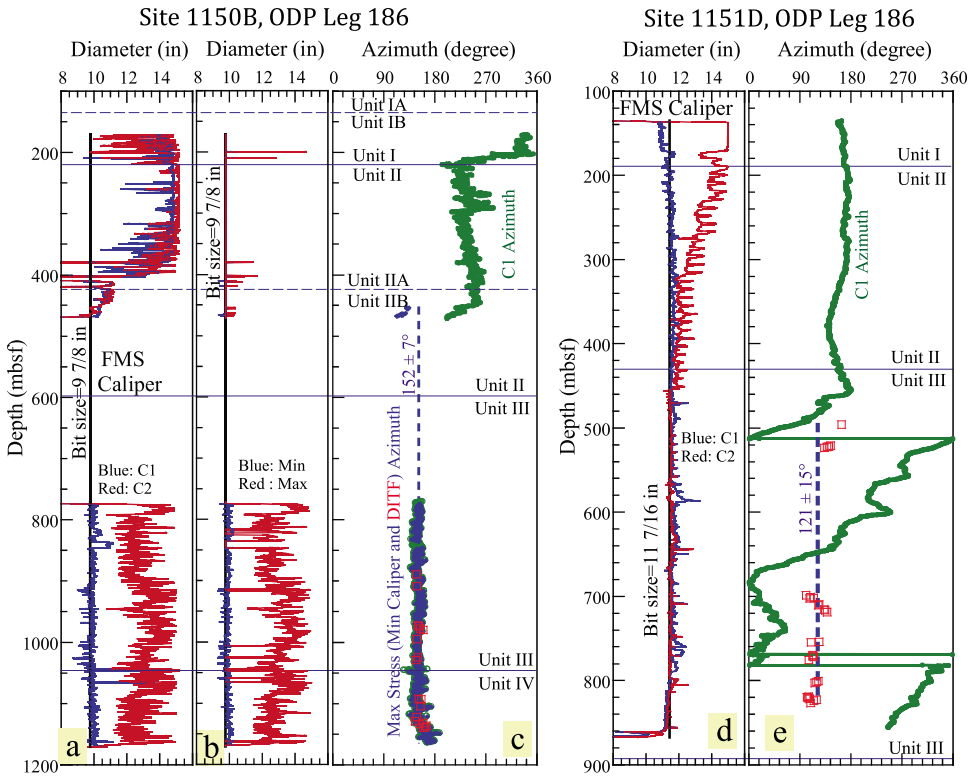

Figure 3. Caliper records and stress orientation at boreholes 1150B and 1151D. (a) Raw FMS caliper data in terms of two borehole diameters in orthogonal directions, labeled C1 and C2, every 6 inches (~15 cm) from 1150B. (b) Selected FMS caliper data meeting the three quality criteria given in the text. (c) C1 azimuth (green dots and line) of FMS caliper and azimuth of the maximum principal horizontal stress from breakouts (blue dots) determined by the selected data shown in Figure 3b except the data rejected by image observation, and from DITFs (red squares) picked up from the FMS images. The average azimuth value and its standard deviation of the maximum principal horizontal stress from both breakouts and DITFs was N152°E ± 7°. (d) Raw caliper data C1 and C2 from 1151D. The spikes shown in the two diameters, especially in C2, might be cause by pipe-tripping operation [*Shipboard Scientific Party*, 2000c]. (e) Azimuths of C1 and the maximum principal horizontal stress from DITFs (red squares) and their average value and standard deviation (N121°E ± 15°).

early Pliocene). In units IB and IIA, the borehole wall had heavy washouts at all azimuths (Figures 2a and 3a) due to the soft and weak sediments. These washouts might also be caused by circumferential stress that exceeded the compressive strength of the sediments, but we could not determine an azimuth for maximum or minimum circumferential stresses. Around the boundary between units IIA and IIB, P wave velocity increased with depth, indicating that sediment strength increased [*Shipboard Scientific Party*, 2000b]. As a result, several breakouts were recognized around 450 mbsf (Figure 2b). Below 775 mbsf (unit III, 598–1047 mbsf, early Pliocene to late Miocene, and unit IV, below 1047 mbsf, late Miocene), widespread breakouts occurred and several DITFs were recognized (Figure 2c).

[15] The caliper data showed that in the Pass 2 logging range (units III and IV) one of the two orthogonal diameters (C1) was almost equal to the bit size, indicating that the borehole wall in this depth range had no failures (Figure 3a). The other diameter (C2) was greater than the bit size (12–14 inches, 30–35 cm), showing clear borehole elongations and suggesting the presence of breakouts. These features suggest that one pair of the FMS caliper arms (C2 in this case) always found the maximum elongated position.

[16] In identifying breakouts from the four-arm caliper data, we used the three criteria used by *Lin et al.* [2010] for controlling data quality. First, the larger caliper diameter should exceed the smaller diameter such that the difference between them is at least 0.05 times the drilling diameter D, in this case approximately 12.5 mm or 0.5 inch for borehole 1150B. Second, the smaller caliper diameter should not exceed 1.05 D. Third, both diameters should not be significantly less than the bit diameter, that is, C1 and C2 > 0.95 D. Seventy-one of the 1976 caliper measurements in the shallower part and 2388 of the 2628 measurements in the deeper part met these criteria (Figure 3b). We rejected twenty-six measurements from around 200 and around 400 mbsf, which satisfied the three criteria for breakout selection but appeared in the FMS imagery to be washouts rather than breakouts.

[17] We determined the profile of maximum principal horizontal stress azimuths around 450 mbsf and from 775 to 1165 mbsf by adding 90° to the minimum principal horizontal stress azimuths as determined from the orientation of maximum borehole elongation in the selected caliper data (blue dots in Figure 3c). Nineteen azimuths of DITFs (each at least 1 m long), representing the maximum principal horizontal stress azimuth, were determined from the depth range of 900–1150 mbsf (red squares in Figure 3c). The azimuth values obtained from breakouts (in caliper data) and DITFs (in FMS images) were in good agreement with each other. The average maximum principal horizontal stress

azimuth at borehole 1150B and its standard deviation were N152°E and 7°, respectively. Azimuth variations (~20°) were recognized around 450 mbsf and 1150 mbsf.

3.2. Borehole 1151D

[18] FMS logging was carried out in a depth range from 135 to 867 mbsf in borehole 1151D in geologic units I, II, and III, which were defined identically with borehole 1150B but at slightly different depth ranges. Borehole elongation (C2 > C1) was clearly recognized above about 400 mbsf (Figure 3d). Three columns of FMS images showed that the borehole walls were complete, but the fourth column showed a mechanically damaged borehole wall (Figure 2d). Therefore, the elongations did not represent breakouts, but might instead have been scratches made during the lowering or raising of drilling pipes. At depths below about 450 mbsf, the caliper data showed that the two orthogonal diameters were almost identical, suggesting that almost no breakouts occurred (Figure 3d). Moreover, the azimuth data show that the FMS arms rotated freely in the borehole over this depth range (Figure 3e), consistent with a circular borehole shape. FMS imagery also showed that the borehole wall was complete in all four positions (Figure 2f). Therefore, no breakouts were recorded in borehole 1151D.

[19] We located 30 DITFs from FMS imagery and measured their azimuths (Figure 3e). The resulting average maximum principal horizontal stress orientations and their standard deviations were N121°E and 15°, respectively.

4. Discussion and Conclusions

[20] The orientations of maximum principal horizontal stress at ODP sites 1150 and 1151, determined from FMS logging conducted in 1999, are interpreted as the stress state prior to the 2011 Tohoku-Oki earthquake. The drilling sites are located on the deep-sea terrace of the Japan Trench about 100 km north-northeast of the epicenter of the mainshock and overlie the coseismic slip zone. The drilling reached approximately 1 km depth, about 10 km above the gently dipping plate boundary that ruptured during the Tohoku-Oki earthquake.

[21] The maximum principal horizontal stress orientation at site 1151, N121°E ± 15°, was parallel to the plate convergence direction and is considered a reasonable reflection of tectonic stress in a plate margin during an interseismic period (Figures 1a and 1b). Unlike site 1151, where only rare microearthquakes occurred before the drilling, site 1150 was within a seismically active zone where microearthquakes have been frequent and M7 earthquakes have been known to recur (Figure 1b) [*Sacks and Suyehiro*, 2003]. Similarly, the degree of interseismic interplate coupling (locking) between the subducting Pacific plate and the overriding Okhotsk plate was lower at site 1150 than at site 1151 (Figure 1a). Because of these differences in seismic characteristics and locking, the stress orientations at the sites differed by about 30°. It might be considered that the stress state at site 1150 reflects local features rather than the far-field tectonic stress. The 30° clockwise rotation of stress orientation at site 1150 relative to the plate motion direction (and site 1151 stress orientation) might reflect lower interplate coupling as the result of the active seismicity.

[22] In the lower parts of the two boreholes, approximately deeper than 500 and 900 mbsf in boreholes 1151D and 1150B, respectively, presence of DITFs might imply that the stress states there had to be reverse or strike-slip faulting stress regimes based on geomechanics considerations [*Zoback*, 2007]. In addition, most of the several hundred earthquakes before the mainshock of 2011 earthquake were of reverse faulting focal mechanisms having a P-axis parallel to the plate convergence direction, and reveal that the stress state before the mainshock was of reverse faulting stress regime although the hypocenters of the earthquakes were much deeper than the drillings [*Hasegawa et al.*, 2011; *Nettles et al.*, 2011]. *Wang and Suyehiro* [1999] also mentioned that stress state in the upper plate in Northeast Japan is in compression detected by numerical simulation.

[23] Focal mechanisms of aftershocks in the hanging wall of the ruptured plate boundary and other coseismic rupturing models indicate a normal faulting postseismic stress regime [*Asano et al.*, 2011; *Kato et al.*, 2011]. Seafloor geodetic observations after the 2011 earthquake show that the co-seismic horizontal displacement of the seafloor in the forearc basin reached 15–24 m being dependent on locations to the east-southeast [*Sato et al.*, 2011], and measurements of local benchmark displacements by acoustic ranging show that the average coseismic horizontal displacement of the frontal wedge was 74 m to the east-southeast [*Ito et al.*, 2011]. Combination of these observations suggests that the coseismic deformation in the hanging wall is definitely extension in the opposite direction of convergence, that is, the stress state might be that of a normal faulting stress regime.

[24] The typical stress orientation before the earthquake, represented by our results from site 1151, shows that the stress state clearly changed with the occurrence of the 2011 Tohoku-Oki earthquake. To take the other stress data before the M_w9.0 mainshock from the focal mechanisms and the numerical simulation into considerations, it is reasonable to conclude that the stress state changed from a reverse faulting to a normal faulting stress regime during the 2011 earthquake sequence. Moreover, *Kato et al.* [2011] concluded a similar stress change pattern during the 2011 earthquake in the Ibaraki segment based on focal mechanism analyses.

[25] **Acknowledgments.** This research used data provided by ODP. Discussion with John Townend (Victoria Univ., New Zealand) and Rob Harris (Oregon State Univ., US) were helpful for finding breakouts in the ODP Leg 186 reports. We gratefully acknowledge the two reviewers, Timothy Byrne and Chandong Chang, for their careful reading and constructive comments which helped us to improve this manuscript. Part of this work was supported by Grants-in-Aid for Scientific Research 22403008 (Japan Society for the Promotion of Science), and 21107006 (Ministry of Education, Culture, Sports, Science and Technology), Japan.

[26] The Editor thanks Chandong Chang and Timothy Byrne for their assistance in evaluating this paper.

References

Asano, Y., T. Saito, Y. Ito, K. Shiomi, H. Hirose, T. Matsumoto, S. Aoi, S. Hori, and S. Sekiguchi (2011), Spatial distribution and focal mechanisms of aftershocks of the 2011 off the Pacific coast of Tohoku earthquake, *Earth Planets Space*, in press.

Avouac, J. P. (2011), The lessons of Tohoku-Oki, *Nature*, *475*, 300, doi:10.1038/nature10265.

Hasegawa, A., K. Yoshida, and T. Okada (2011), Nearly complete stress drop in the 2011 Mw9.0 off the Pacific coast of Tohoku earthquake, *Earth Planets Space*, in press.

Hino, R., S. Ito, H. Shiobara, H. Shimamura, T. Sato, T. Kanazawa, J. Kasahara, and A. Hasegawa (2000), Aftershock distribution of the 1994 Sanriku-oki earthquake (Mw 7.7) revealed by ocean bottom

seismographic observation, *J. Geophys. Res.*, *105*, 21,697–21,710, doi:10.1029/2000JB900174.

Ide, S., A. Baltary, and G. C. Beroza (2011), Shallow dynamic overshoot and energetic deep rupture in the 2011 Mw 9.0 Tohoku-Oki earthquake, *Science*, *332*, 1426–1429, doi:10.1126/science.1207020.

Ito, Y., T. Tsuji, Y. Osada, M. Kido, D. Inazu, Y. Hayashi, H. Tsushima, R. Hino, and H. Fujimoto (2011), Frontal wedge deformation near the source region of the 2011 Tohoku-Oki earthquake, *Geophys. Res. Lett.*, *38*, L00G05, doi:10.1029/2011GL048355.

Kato, A., S. Sakai, and K. Obara (2011), A normal-faulting seismic sequence triggered by the 2011 off the Pacific coast of Tohoku earthquake: Wholesale stress regime changes in the upper plate, *Earth Planets Space*, in press.

Lin, W., et al. (2010), Present-day principal horizontal stress orientations in the Kumano forearc basin of the southwest Japan subduction zone determined from IODP NanTroSEIZE drilling Site C0009, *Geophys. Res. Lett.*, *37*, L13303, doi:10.1029/2010GL043158.

Maeda, T., T. Furumura, S. Sakai, and M. Shinohara (2011), Significant tsunami observed at the ocean-bottom pressure gauges at 2011 off the Pacific coast of Tohoku earthquake, *Earth Planets Space*, in press.

Nettles, M., G. Ekström, and H. C. Koss (2011), Centroid–moment-tensor analysis of the 2011 Tohoku earthquake and its larger foreshocks and aftershocks, *Earth Planets Space*, in press.

Ozawa, S., T. Nishimura, H. Suito, T. Kobayashi, M. Tobita, and T. Imakiire (2011), Coseismic and postseismic slip of the 2011 magnitude-9 Tohoku-Oki earthquake, *Nature*, *475*, 373–376, doi:10.1038/nature10227.

Sacks, I. S., and K. Suyehiro (2003), Chapter 1, Leg 186 synthesis: Drilling the forearc of the northeast Japan arc—Causes and effects of subduction plate coupling over 20 m.y., edited by K. Suyehiro et al., *Proc. Ocean Drill. Program Sci. Results*, *186*, 1–27.

Sato, M., T. Ishikawa, N. Ujihara, S. Yoshida, M. Fujita, and A. Asada (2011), Displacement above the hypocenter of the 2011 Tohoku-Oki earthquake, *Science*, *332*, 1395, doi:10.1126/science.1207401.

Shipboard Scientific Party (2000a), Chapter 1, Leg summary, edited by I. S. Sacks et al., *Proc. Ocean Drill. Program Init. Rep.*, *186*, 1–37.

Shipboard Scientific Party (2000b), Chapter 4, Site 1150, edited by I. S. Sacks et al., *Proc. Ocean Drill. Program Init. Rep.*, *186*, 1–209.

Shipboard Scientific Party (2000c), Chapter 5, Site 1151, edited by I. S. Sacks et al., *Proc. Ocean Drill. Program Init. Rep.*, *186*, 1–125.

Suyehiro, K., and A. Nishizawa (1994), Crustal structure and seismicity beneath the forearc off northeastern Japan, *J. Geophys. Res.*, *99*, 22,331–22,347, doi:10.1029/94JB01337.

Tsuru, T., J.-O. Park, N. Takahashi, S. Kodaira, Y. Kido, Y. Kaneda, and Y. Kono (2000), Tectonic features of the Japan Trench convergent margin off Sanriku, northeastern Japan, revealed by multichannel seismic reflection data, *J. Geophys. Res.*, *105*, 16,403–16,413, doi:10.1029/2000JB900132.

Wang, K., and K. Suyehiro (1999), How does plate coupling affect crustal stresses in northeast and southwest Japan?, *Geophys. Res. Lett.*, *26*, 2307–2310, doi:10.1029/1999GL900528.

Zoback, M. D. (2007), *Reservoir Geomechanics*, Cambridge Univ. Press, New York, doi:10.1017/CBO9780511586477.

Zoback, M. D., C. A. Barton, M. Brudy, D. A. Castillo, T. Finkbeiner, B. R. Grollimund, D. B. Moos, P. Peska, C. D. Ward, and D. J. Wiprut (2003), Determination of stress orientation and magnitude in deep wells, *Int. J. Rock Mech. Min. Sci.*, *40*, 1049–1076, doi:10.1016/j.ijrmms.2003.07.001.

Y. Hashimoto, Department of Applied Science, Kochi University, 2-5-1 Akebono-cho, Kochi 780-8520, Japan.

T. Kanamatsu, S. Saito, and Y. Yamamoto, Institute for Research on Earth Evolution, Japan Agency for Marine-Earth Science and Technology, 2-15 Natsushima-cho, Yokosuka, Kanagawa 237-0061, Japan.

W. Lin, Kochi Institute for Core Sample Research, Japan Agency for Marine-Earth Science and Technology, 200 Monobe-otsu, Nankoku, Kochi 783-8502, Japan. (lin@jamstec.go.jp)

Y. Sanada, Center for Deep Earth Exploration, Japan Agency for Marine-Earth Science and Technology, 3173-25 Showa-machi, Kanazawa-ku, Yokohama, Kanagawa 236-0001, Japan.